Article

Determination of ASR in Concrete Using Characterisation Methods

Murat Doğruyol *

Posted Date: 5 January 2024

doi: 10.20944/preprints202401.0494.v1

Keywords: Basalt aggregate; limestone aggregate; fly ash; concrete; XRD; TGA-DTA

Article

Determination of ASR in Concrete Using Characterisation Methods

Murat Doğruyol *

Department of Civil Engineering, Siirt University, 56100, Siirt, Turkey; mdogruyol@siirt.edu.tr

Abstract: Alkali-Silica Reaction (ASR), which develops over time into a harmful internal reaction in concrete, produces a harmful gel due to the reaction between the reactive silica in the aggregate and the alkalis of the pore solution. Due to the multi-scale nature of this long-term phenomenon, understanding its mechanism in concrete structures remains difficult to assess. Accelerated Mortar Bar Testing (AMBT) ASTM C1260 is among the commonly used methods to understand ASR formation in a short time. In this study, the chemical characterisation of concretes produced from volcanic rock type basalt aggregate was compared with the chemical characterisation of ASR concretes after AMBT was applied. In addition, 20% FA was substituted into the concrete to investigate the effect of fly ash (FA) on ASR. Specimens with limestone aggregate (PL), basalt aggregate (BBC) and 20% basalt aggregate with fly ash substitution instead of cement (BBC20FA) were prepared for the investigation. Scanning electron microscopy (SEM), energy dispersive X-ray spectrometry (EDX), X-ray diffraction (XRD), Fourier transform infrared spectroscopy (FT-IR), thermogravimetric analysis (TGA) and differential thermal analysis (DTA) techniques were used to characterise the morphology and analytical composition of the concretes. It was determined that basalt aggregate does not cause ASR and its use with fly ash increases the strength and durability of concrete.

Keywords: Basalt aggregate; limestone aggregate; fly ash; concrete; XRD; TGA-DTA

1. Introduction

Concrete is a composite building material consisting of cement, water and aggregate. Aggregate constitutes approximately 70% of the concrete volume [1]. Dolomite and limestone are widely used and basalt is limitedly used as concrete aggregate. The results of some tests on basalt aggregate concretes conducted in the middle of the 20th century showed that basalt rocks were superior to other rocks. Aggregate size, mechanical and chemical properties play an active role in the strength of concrete [1,2]. In addition to the physical and mechanical properties, the chemical properties of the aggregate used in concrete must meet certain conditions without any harmful components [3–9].

Aggregates containing reactive silica such as andesite, dacite, rhyolite, basaltic andesite and cement and alkalis (Na_2O, K_2O) in the environment and the effect of moisture and alkali-aggregate reaction are formed. The gelatinous structure formed as a result of alkali-aggregate reaction creates significant cracks and reduces the strength and durability of concrete (Figure 1). ASR gel can cause slow but severe internal degradation in concrete structures [3–9].

An accelerated test method such as ASTMC 1260 is one of the methods applied to evaluate the reactivity of the aggregate to ASR. In addition, observation of microstructure with scanning electron microscope with SEM/EDX and elemental changes in concrete specimens are the methods used to understand ASR [3,4,9].

According to SEM/EDX, silicon, alkalis and calcium constitute the majority of ASR products formed in aggregates, characterized by atomic ratios of (Na + K)/Si ≈ 0.25 and Ca/Si ≈ 0.25. [10,11]. ASR products were synthesised at 40 °C to gain a better understanding of the structure, expansion behavior, and formation conditions of ASR products formed in field concrete. In 100 mL rigid polyethylene (PE-HD) bottles, specimens were prepared by combining 6.008 g hydrophilic silica, 1.402 g freshly burned CaO, 2.805 g analytical KOH (≥85% KOH base), and 50 mL Milli-Q water.

Preprints (www.preprints.org) | NOT PEER-REVIEWED | Posted: 5 January 2024 doi:10.20944/preprints202401.0494.v1

Following 160 and 210 days of storage at 40 °C, the specimens underwent filtering and drying. In addition to the usual rosette or plate-like morphology, the SEM image acquired for the vacuum-dried specimen in Figure 1 displays ASR products with narrower plate-like and even rod-like morphologies [12].

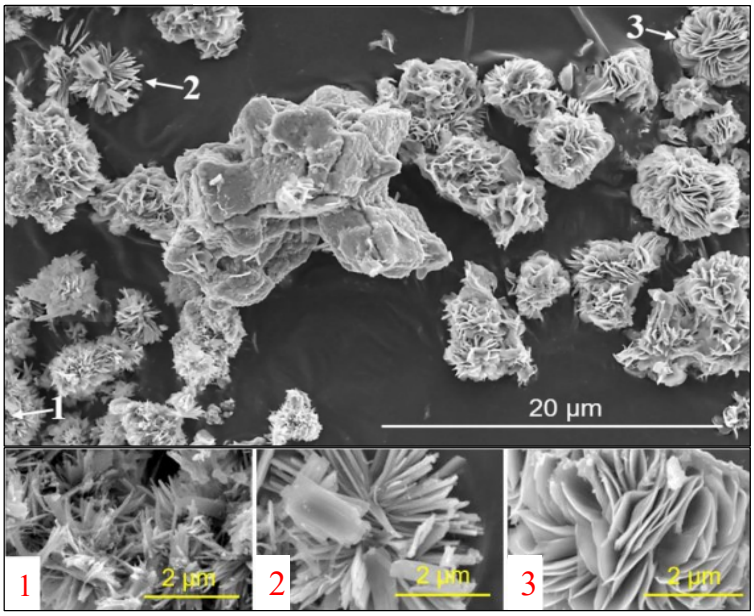

Figure 1. SEM image of the ASR product synthesized by keeping it at 40 °C for 160 days [12].

The crystal structure of the ASR product can be determined despite the poor clarity of the diffraction patterns caused by the comparatively low crystallinity of nano-sized ASR particles. According to each crystal phase's particular atomic arrangement, the chemical alteration of each crystal phase was examined using the X-ray diffraction method (XRD) on the basis of X-rays diffracting in a distinctive order [12]. ASR products developed in the field and synthetically produced gels have similar formations [13]. The reflection that is highest at $2\theta \approx 26^{o}$ might be related to the typical reflection seen in amorphous silicates between 24^{o} and 31^{o} [14].

1.1. Effect of ASR on Durability of Concrete

The alkali-aggregate reaction has been the subject of research since the mid-1930s, following the discovery of the alkali-silica reaction (ASR) by Thomas Stanton of the California Highway Department. However, the fact that ASR is both amorphous and crystalline has led to a lack of understanding of reaction mechanisms, test methods, prediction and diagnosis [15].

Alkali silica reaction (ASR) is a form of concrete deterioration that occurs as a result of the reaction of the SiO_2 in the reactive aggregate present in the aggregates used in concrete additives with the Na_2O and K_2O (alkali) components that make up the cement. The formation of ASR gel has been reported to increase the volumetric expansion in the concrete and create superficial cracks, thus reducing the strength and durability of the concrete. It has been determined that the use of mineral additives such as fly ash and silica fume reduces the formation of cracks due to ASR and increases the strength and durability of concrete [6,8,16–29]. ASR formation mechanism is given in Figure 2. Reactions caused by ASR take place in two stages [4].

$$\underset{\text{(Reactive silica) + (alkali)}}{H_{0.38}SiO_{2.19} + 0.38\,NaOH} \rightarrow \underset{\text{(Alkali silica gels) + (water)}}{Na_{0.38}SiO_{2.19} + 0.38\,H_2O} \quad (1)$$

$$\underset{\text{(Alkali silica gels) + (alkali)+ (moisture)}}{SiO_{2.19} + 1.62NaOH + 0.38\,H_2O} \rightarrow \underset{\text{(Alkaline silicate hydrate gel)- (Expansion)}}{2Na^{+}H_2SiO_2^{-4}} \quad (2)$$

Preprints (www.preprints.org) | NOT PEER-REVIEWED | Posted: 5 January 2024 doi:10.20944/preprints202401.0494.v1

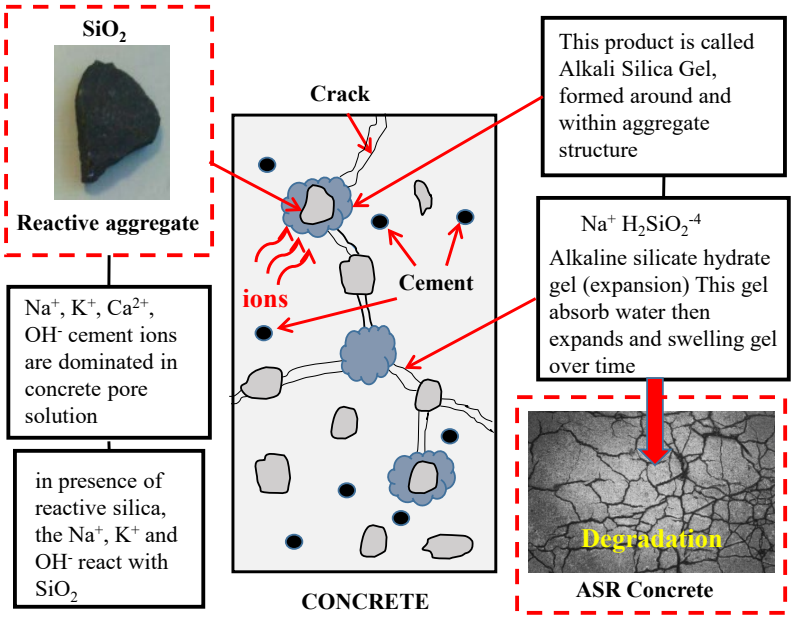

Figure 2. The ASR mechanism schematic for concrete structures.

1.2.1. Reactive Aggregates

The chemical structure of the aggregate forming the concrete is important in terms of durability. Bérubé and Ferruce (1994), in their study, have reported andesite, chert, opal, tridymite, cristobalite, acidic basalt, and dacite as reactive rocks that cause ASR expansion [30]. On the other hand, they have reported that rocks such as Dolomite, limestone, chalcedony, quartz caused alkali-carbonate reaction (ACR) expansion, not ASR. Classification of rocks is given in Figure 3 [31].

It is known that the physical structure of the aggregate also affects the ASR reactivity. It has been determined that the coarse aggregate is more reactive to ASR than the fine aggregate, and the porosity of the aggregate particles increases the ASR expansion rate [16,17,32].

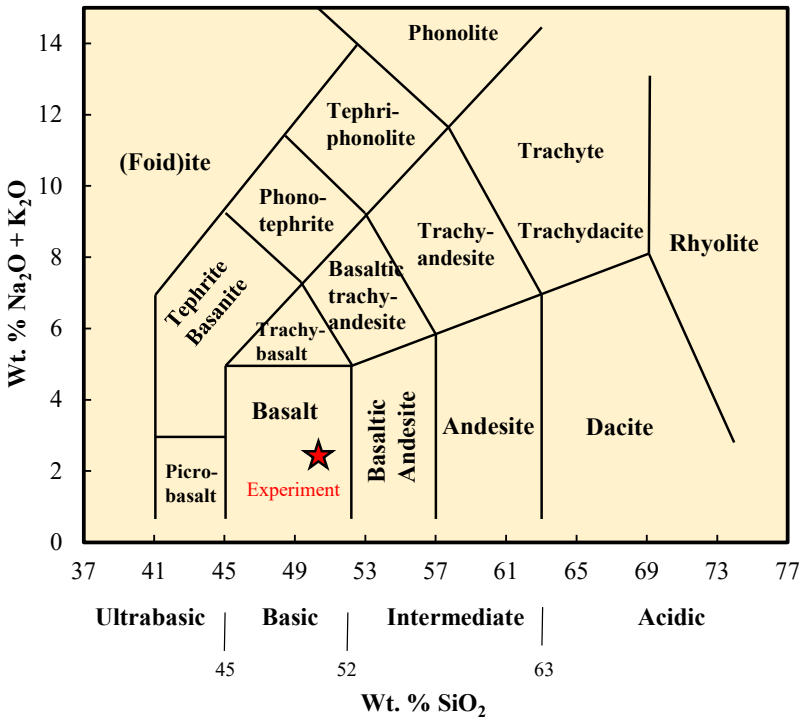

Figure 3. Classification of volcanic rocks (SiO_2 - Na_2O+K_2O TAS diagram) [31].

Preprints (www.preprints.org) | NOT PEER-REVIEWED | Posted: 5 January 2024 doi:10.20944/preprints202401.0494.v1

1.2.2. Alkalinity of cementations materials

Recent research has categorised cements as low alkaline (Na_2O content 0.5%) or high alkaline (Na_2O content 1.04%). To counteract ASR, highly reactive rocks should only be used in combination with low alkaline cements [1,3–8].

Although cement contains various alkali metals, sodium Na+ and potassium K+ ions play an important role in ASR concrete deterioration [3–6].

The formula used to calculate the alkali content of cement is presented below [22].

$$Na_2Oeq = Na_2O + 0.658K_2O < \%0.6 \quad (3)$$

In the previous study [9], it was found that the use of basalt aggregate, silica fume and fly ash increased sulphate resistance by reducing the volumetric expansion of concrete [9,33]. Fly ash can be used instead of cement due to the closeness of its Blaine value to the cement, and its content of SiO_2, AlO_3, FeO, which are chemical components of the cement. Fly ash (FA) transforms into Calcium-Silicate-Hydrate (C-S-H), which binds to Calcium Hydroxide (CH) from hydration products thanks to its silicate content and increases its strength over time. Thus, it contributes to the reduction of the ratio of CH and C_3A in the binder. In addition, it has been reported that fly ash, which is substituted for cement at a rate of 20%, reduces the CaO/SiO_2 ratio in the mixture, strengthens the C-S-H bond, and increases the resistance of the concrete against the expansion failures due to ASR by reducing the amount of sulphate attacks and alkaline in the environment [9,33,34].

This study aims to discuss the mechanisms of ASR-related products using characterization analyses such as SEM-EDS, XRD and FT-IR after applying the conventional AMBT method to determine the ASR reactivity of silicate-containing concrete aggregate and Portland cement. This study is important because it shows the effect of FA substitution in concrete and the chemical content of the aggregate rock on concrete durability.

2. Materials and Methods

2.1. Materials

CEM I 42.5 N Portland cement (ASTM C type I) with a density of 3.15 g/cm^3, Blaine specific surface of 387 m^2/kg and Class C fly ash (FA) with a density of 2.20 g/cm^3, Blaine specific surface of 217 m^2/kg were used in the experiment. The specific surface areas of the materials were measured in accordance with EN 196:6 and ASTM C 204 standards [35,36]. The analysis results of fly ash and Portland cement were conducted at Limak Ergani Cement Plant (Limak Holdings Inc., Ankara, Turkey). Table 1 shows the chemical composition of Portland cement and FA. Table 2 shows mineralogical composition of Portland cement. Table 3 shows the physical and mechanical properties of used aggregate.

Table 1. Chemical composition by XRF of the materials (wt. %).

	SiO_2	Al_2O_3	Fe_2O_3	CaO	$CaCO_3$	MgO	SO_3	Na_2O	K_2O	LOI[1]	Na_2Oeq^*
Cement	18.12	5.21	3.03	62.06	-	2.70	3.21	0.09	0.96	3.98	0.72
FA	21.65	33.55	8.76	27.50		4.50	0.05	0.84	1.76	1.29	2.00
Basalt	50.63	10.51	6.49	-	21.55	3.32	-	0.45	1.63	2.08	2.08

[1]LOI: Loss on ignition; $Na_2Oeq^* = Na_2O + 0.658\ K_2O$

Table 2. Mineralogical composition of Portland cement (wt. %).

$3CaO.SiO_2$ (C_3S)	$2CaO.SiO_2$ (C_2S)	$3CaO.Al_2O_3$ (C_3A)	$4CaO.Al_2O_3.Fe_2O_3$ (C_4AF)
66.40	1.87	8.68	9.22

Table 3. Properties of the coarse basalt aggregate.

	Acceptance limits

Preprints (www.preprints.org) | NOT PEER-REVIEWED | Posted: 5 January 2024 doi:10.20944/preprints202401.0494.v1

Compressive Strength (MPa)	92	
Schmidt hammer (MPa)	50	
Water absorption (%)	2.70	< 3.0 [37]
LA Abrassion loss (%)	27	< 50 (500 cycles) [38]
Density (g/ cm^3)	2.78	< 2.70 [39]

In order to classify igneous rocks, samples were taken from the central parts of Cizre, Şırnak (Southeast of Turkey) and all samples shared the same fundamental features [31]. The mineralogy, petrography and petrology of the volcanics of the Cizre region used in the experiment, whose X-ray Fluorescence (XRF) analysis is given in Table 1, were determined as basalt according to Figure 3. According to Table 1, Due to its low SiO_2 concentration, which is less than 51%, the chemical studies of the Cizre basalt specimens demonstrate that it is basic and unlikely to be a reactive aggregate to ASR [6].

The temperature at which the fly ash burns and the cooling rate determine how the particles will appear [40]. Most of the Particles observed in the study were solid spheres ranging in size from about 1 to 100 μm. SEM image of fly ash and Portland cement is given in Figure 4 and XRD analysis is given in Figure 5.

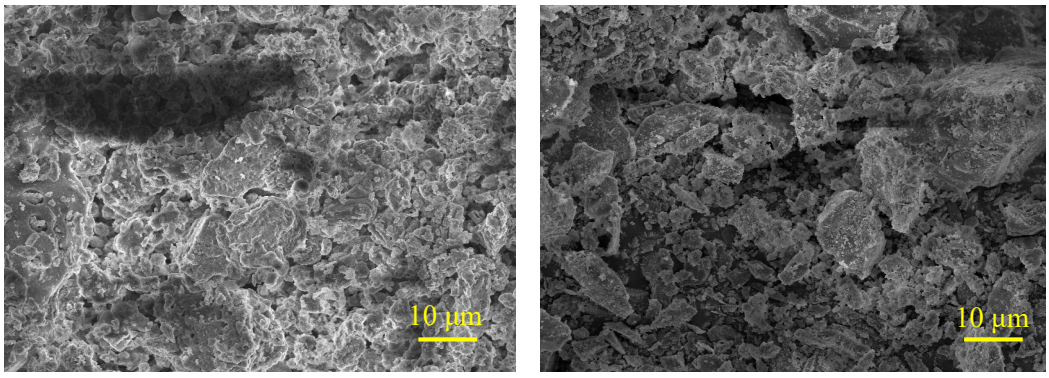

Figure 4. a) fly ash b) Portland cement SEM image.

Fly ash the absence of a hump or "halo" around the sharp broad peak centred at approximately 25.49° 2θ in the diffractogram indicates that the fly ash is Class C [41]. Class C fly ash is normally produced from lignite and lower bituminous coals and usually contains significant amounts of calcium hydroxide or lime [42] . In the XRD analysis of Portland cement, C_3S, C_2S, C_3A and C_4AF were detected as the main components, and it is seen that the XRD pattern of the cement has a crystalline structure suitable for a typical Portland cement.

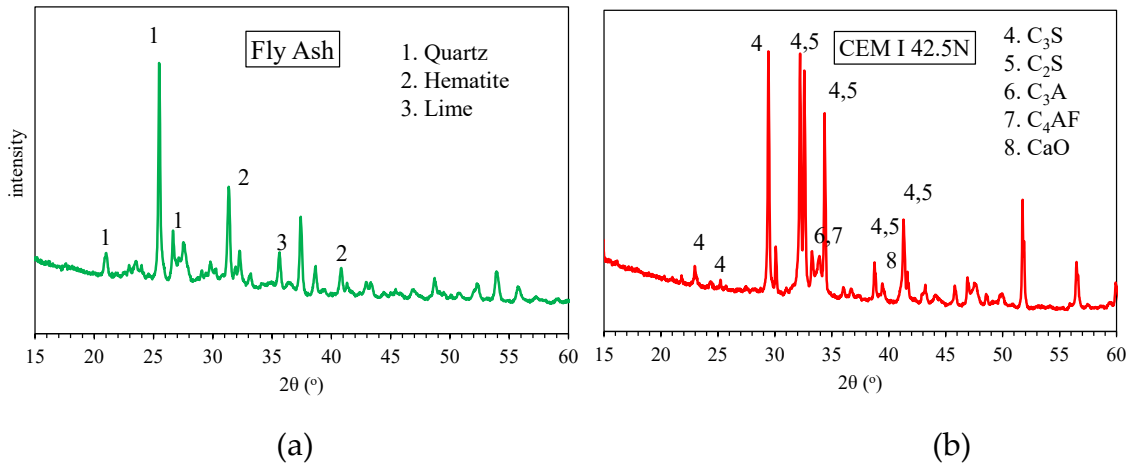

Figure 5. a) fly ash b) Portland cement XRD analyses.

Preprints (www.preprints.org) | NOT PEER-REVIEWED | Posted: 5 January 2024 doi:10.20944/preprints202401.0494.v1

Class C fly ash differs from Class F fly ash primarily by having a higher calcium content. Previous studies have noted that much of the literature is on the activation of low-calcium fly ashes, where calcium is primarily considered as a contaminant that produces various hydrate[43,44] assemblages that can cause a decrease in strength [45]and a slowing of the reaction rate [46]. However, some studies have revealed that Class C fly ash has both pozzolanic and cementitious qualities [42].

2.2. Preparation of Specimens

For testing, 25 mm x 25 mm x 285 mm (1 in x 1 in x 11.25 in) mortar specimens were manufactured to ASTM C150 standard aggregate gradation. As part of the test protocol, the specimens were fully immersed in 1 M NaOH solution for 14 days at 80 °C (176 °F). Specimens prepared in accordance with ASTMC 1260 standards were tested in the construction laboratory of TSI (Turkish Standards Institute), and the elongation of the mortar rods was determined. The specimens were brought into a suitable form for the characterisation methods. Then, the specimens were brought into a form suitable for characterisation methods. The results obtained from ASR concrete and ASR gel were compared with the results obtained in studies of other authors.

In addition, to determine the effect of the solution on the compressive strength, the BBC and BBC20FA designs prepared for the ASTMC 1260 test were poured into a 4 cm*4 cm*16 cm mortar bar mould. After curing the concrete specimens for 28 days, one group of mortar bars was exposed to hydropath (T = 20 ± 2 °C and R.H. ≈ 95%) and the other group was exposed to ASTMC 1260 test conditions (1M NaOH, 80°C) for 14 days. After 14 days, specimens from the NaOH solution were combined with the other group to better understand the changes in hydration products and the effect of fly ash on concreteThe mortar bars were cut with a concrete cutting saw to obtain 4 cm cube specimens which were then crushed in a cement press to determine the compressive strength values (Figure 6).

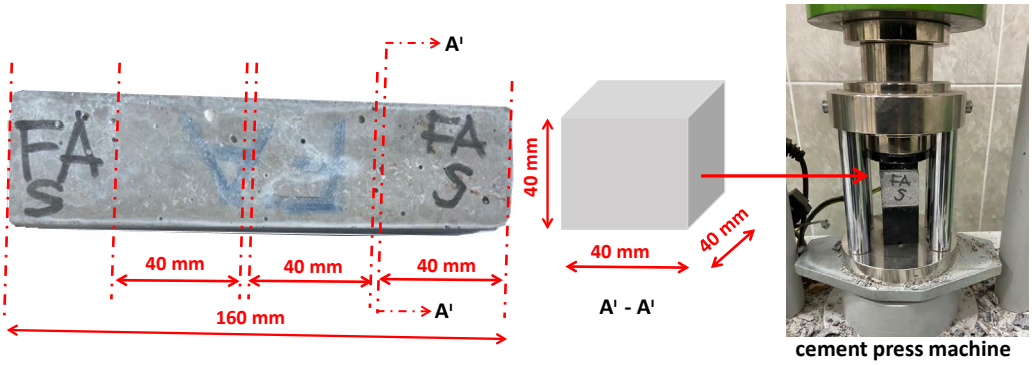

Figure 6. Preparation of specimens for compressive strength test.

Concrete specimens with a water/binder ratio = 0.47 were prepared and placed in a 25x25x285 mm mold as required by ASTMC1260 [47]. Cizre basalt was used as aggregate, Portland cement and fly ash as binder. Specimens were produced with 20 wt% substitution of basalt aggregate (BBC) and fly ash (BBC20FA) instead of cement. For comparison, limestone aggregate was used in PL (Plain) concrete. The mix design of the test specimens is given in Table 3 in the proportions specified by ASTM 1260 [47].

Table 4. Concrete mixture.

	Sieves									
	No:4	No:8	No:16	No:30	No:50					
Specimens	%10	%25	%25	%25	%15					
	Aggregate					C[1]	FA[2]	W[3]	W/B[4]	C/A[5]
	Gram									

Preprints (www.preprints.org) | NOT PEER-REVIEWED | Posted: 5 January 2024 doi:10.20944/preprints202401.0494.v1

PL	99	247.5	247.5	247.5	148.5	440	-	206.8	0.47	2.25
BBC	99	247.5	247.5	247.5	148.5	440	-	206.8	0.47	2.25
BBC20FA	99	247.5	247.5	247.5	148.5	352	88	206.8	0.47	2.25

[1]C=Cement; [2]FA= Fly Ash;[3] W= Water; [4]W/B= Water- Binding ratio; [5]C/A= Cement- Aggregate ratio

2.3. Mechanical Properties

Compressive strength values were calculated by breaking in a YKM-CM106 model press machine calibrated by TURKAK (Turkish Accreditation Agency, Ankara, Turkey) in the construction laboratory of Siirt University (Siirt, Turkey). 50 N/s were loaded at a rate. To confirm the accuracy of the findings, three specimens of each concrete type were analysed and averaged.

2.4. Mineralogical and Chemical Characterisation

The microstructural structure of the mortars is the structure that occurs at the binder/aggregate intersection reactions under SEM can be examined [48]. After confirming existing knowledge, specimens were obtained from the outer edge of each broken specimen for SEM examination to assist understand the mechanisms underlying the strength disparities. The specimens were brought to a suitable form for the SEM device. In order to take images, the surface to be imaged was made conductive with the help of an Au coating device. We placed our specimens in the chamber part of our SEM device. We started our process. SEM analyses were performed at room temperature. Surface morphologies of the specimens were characterized with scanning electron microscopy SEM, LEO-EVO 40 (Cambridge-England) at various scales. For the scanned regions, energy-dispersive X-ray spectroscopy (EDX) using a Bruker-125 eV (Berlin, Germany) was used. A Rigaku RINT-2000 diffractometer was used to record the products' X-ray diffraction patterns. Cu-Kα radiation was applied to the specimens at a voltage of 40 kV and a current of 15 mA. Furthermore, XRD analyses were performed at a wavelength of 1.5406 (λ) between 10° and 90°, scanning at a rate of 2° per minute and with a step speed of 0.02°. The Origin Jasco FT-IR spectrometer was used to recognize the mineralogical characteristics of the mortars, the infrared spectra of mortars specimen was recorded in the region 400–4000 cm^{-1}. The resolution of the instrument is 0.001 cm^{-1} and the accuracy is 74 cm^{-1}. The Origin Jasco FT-IR spectrometer was used to recognize the mineralogical characteristics of the mortars, the infrared spectra of mortars sample was recorded in the region 400–4000 cm^{-1}. The resolution of the instrument is 0.001 cm^{-1} and the accuracy is 74 cm^{-1}. Thermogravimetric analysis (TGA) and differential thermal analysis (DTA) were carried out in a nitrogen atmosphere with a heating rate of 10 °C/min. using Shimadzu DTG60 AH (Shimadzu DSC 60 A) thermal analysers. A sample size of 19– 22 mg was used.

3. Results and Discussion

3.1. Accelerated Mortar Bar Testing (AMBT) ASTM C1260

According to ASTMC 1260, average elongation rate of mortar rods <0.10% non-hazardous aggregate in terms of alkali silica reactivity, 0.10% <mean elongation <0.20% potentially hazardous aggregates, mean elongation rate >0.20% are considered hazardous aggregates [47].

AMBT was carried out by the method of accelerated expansion of mortar bars of alkali-silica reactivity of aggregates. Length change measurements were made at the end of 3, 7, and 14 days. Equation 5 was used to determine the percentages of change in unit length:

$$\text{Mortar bar expansion (L)} = \frac{L_n - L_0}{G} \times 100 \quad (5)$$

Where L is the length change at age "x" days (%), Lo is the initial comparator reading of the specimen less the initial comparator reading of the reference bar (mm), G is the nominal gauge length (285 mm), and Ln is the comparator reading of the specimen at age "x" minus the comparator reading of the reference bar at age "x" (mm). Figure 7 displays changes in length based on ASTM C 1260 standards.

Preprints (www.preprints.org) | NOT PEER-REVIEWED | Posted: 5 January 2024 doi:10.20944/preprints202401.0494.v1

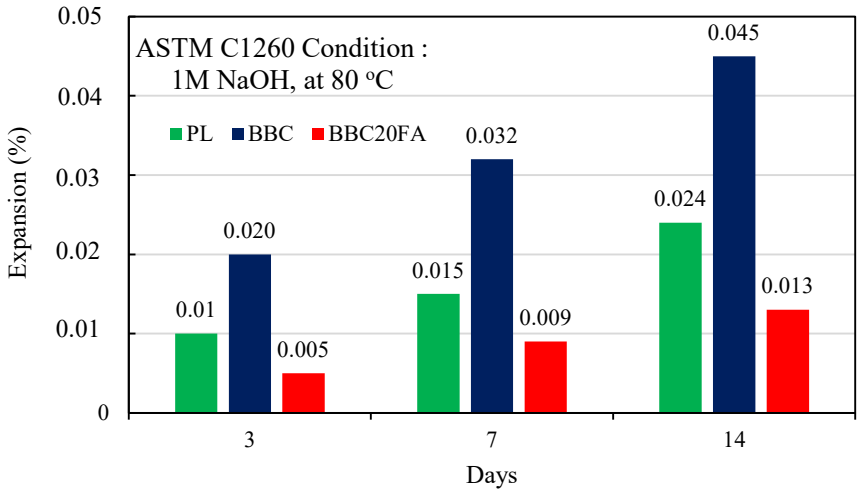

Figure 7. Expansion amounts of specimens according to ASTMC 1260.

According to Figure 7, after 3, 7 and 14 days after AMBT analysis, 0.010%, 0.015%, 0.024% elongation was measured in limestone aggregate concrete (PL), 0.020%, 0.032%, 0.045% elongation was measured in basalt aggregate concrete (BBC), 0.020%, 0.032% and 0.045% elongation was measured in basalt aggregate concrete with 20% fly ash substitution (BBC20FA), respectively.

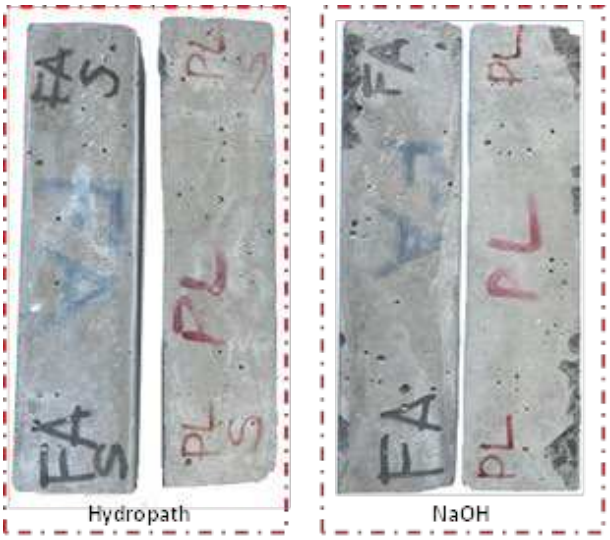

Figure 8. Macro images of BBC (PL) and BBC20FA (FA) bar specimens with curing conditions in (a) hydropath and (b) 1M NaOH at 80°C.

According to Figure 8, when the macro image of the specimens kept in the NaOH solution is examined, the spills on their surfaces are visible to the naked eye (Figure 8b).

3.2. Compressive Strength

Concrete specimens (40x40x160 mm), after 28 days of hydropath, were immersed in 1 M NaOH solution at 80 °C for 14 days and then dried in a drying oven at 105 °C for 4 h. After the specimens prepared for the experiment were kept in hydropathy and NaOH solution, they were turned into 4 cm cubes as shown in Figure 4. The strength of the concrete specimens was tested. The compressive strength values of the specimens are shown in Figure 6. Then, the non-immersed specimen in hydropath was used as a reference and the strength loss rate was determined using Equation 6.

Preprints (www.preprints.org) | NOT PEER-REVIEWED | Posted: 5 January 2024 doi:10.20944/preprints202401.0494.v1

$$CS_L = \frac{CS_N - CS_{PL}}{CS_{PL}} \; x \; 100\% \qquad (6)$$

Where CS_N is the compressive strength of the concrete specimens exposed to a 1M NaOH solution (MPa), CS_{PL} is the compressive strength of the concrete specimens in hydropath (MPa), and CS_L is the percentage loss of the specimen's compressive strength. As a result, the specimens' alkali resistance was determined by measuring their rate of strength loss; a high rate of strength loss indicates poor alkali resistance, whereas a low rate of strength loss indicates good alkali resistance.

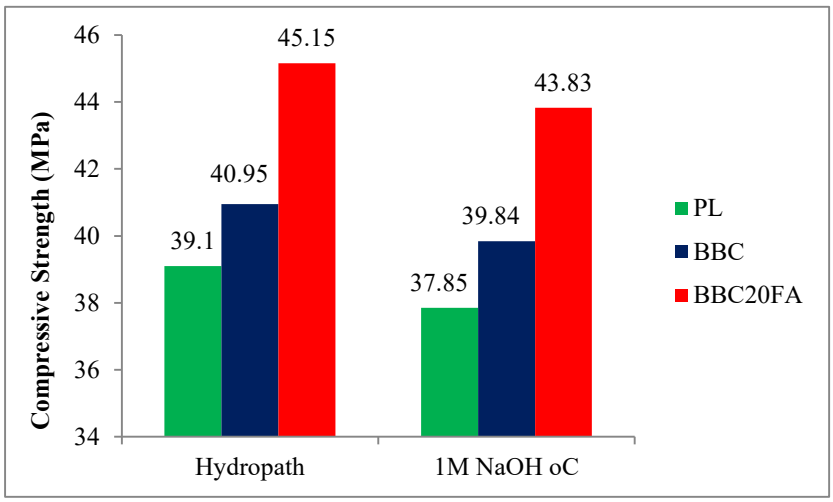

Figure 9. Compressive strength values at the end of 6 weeks.

Figure 9 clearly shows that NaOH solution treated fly ash can; increase the compressive strength of basalt aggregate concrete. Fly ash replacement provided more than 10% increase in strength in both cure conditions. In addition, NaOH solution caused 3.19% 2.79% and 3.01% strength loss in PL, BBC and BBC20FA specimens, respectively Table 5.

Table 5. Compressive strength values and strength losses.

	Hydropath	1M NaOH 80 °C	Strength loss (CS_L),%
PL	39.10 MPa	37.85 MPa	-3.19
BBC	40.95 MPa	39.84 MPa	-2.79
BBC20FA	45.15 MPa	43.83 MPa	-3.01
FAE*	+10.25%	+10.01%	

FAE* = Effect of Fly Ash admixture on compressive strength of concrete

3.3. SEM-EDX analysis

After testing the compressive strength of the specimens exposed to the ASTM C 1260 test, the remaining parts were brought into a suitable form for the examination of their microstructures. In addition to ordinary hydration products such as C-S-H bond, Portlandite and Ettringite Figure 10, ASR-like products Figure 11 with crystalline structure were also observed in the samples. These needle-like products were similar to the crystalline ASR product shown in Figure 1.

Preprints (www.preprints.org) | NOT PEER-REVIEWED | Posted: 5 January 2024 doi:10.20944/preprints202401.0494.v1

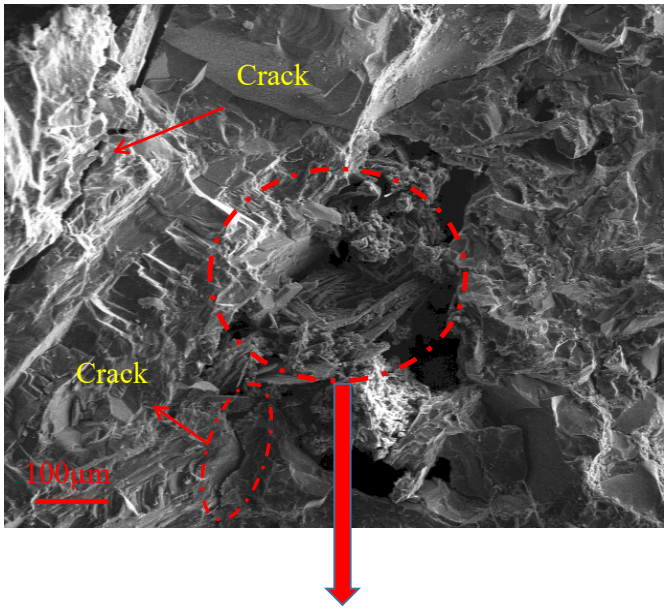

(a)

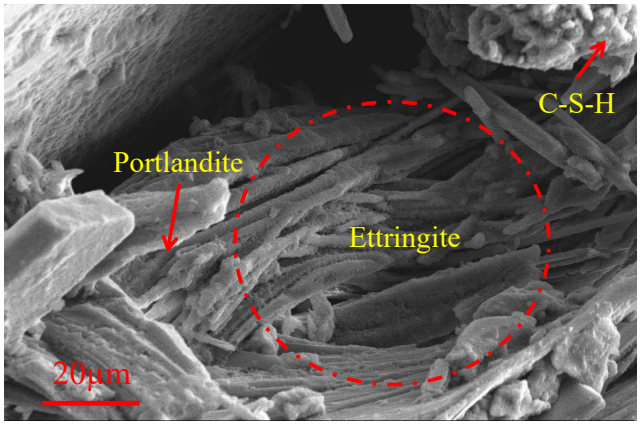

(b)

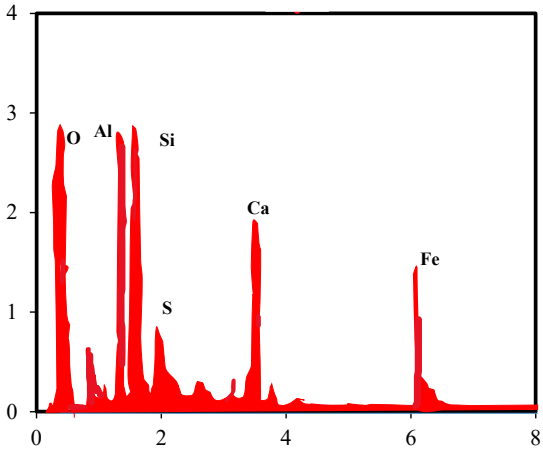

(c)

Figure 10. BBC20FA specimens of a) Macro crack SEM images b) hydration products that cause macro-crack SEM images c) EDX analysis.

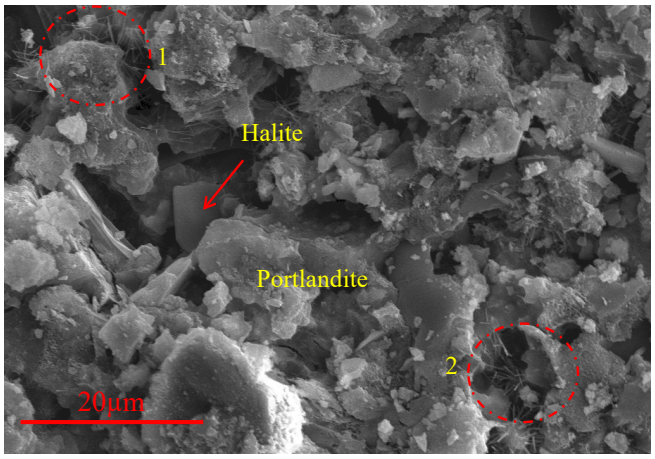

(a)

Preprints (www.preprints.org) | NOT PEER-REVIEWED | Posted: 5 January 2024 doi:10.20944/preprints202401.0494.v1

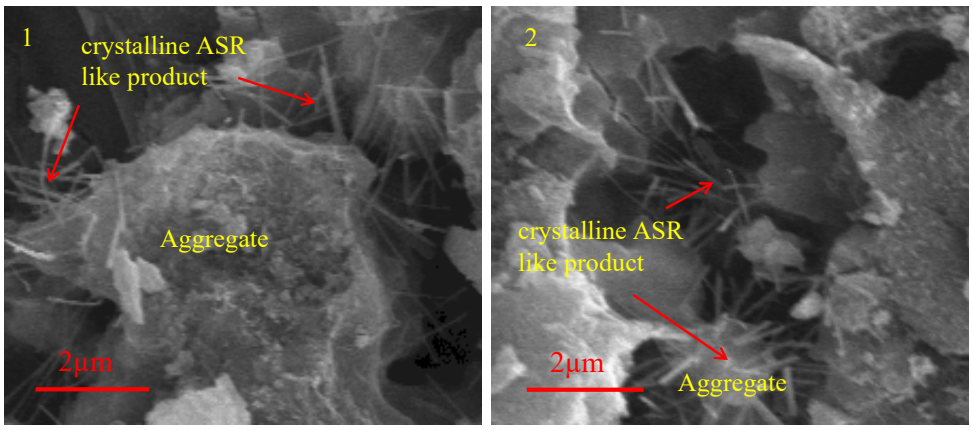

(b) (c)

Figure 11. SEM images of BBC specimen.

When sufficient calcium (Ca^{2+}) is present in the hydration products, expansion occurs and is in the form of portlandite. Expansion is caused by the development of calcium-rich gels. Furthermore, calcium increases the viscosity of the formed gel, causing it to grow. In contrast, several investigations have indicated that adding CaO to concretes containing fly ash or silica fume lowers expansion [45,46]. It has been determined that the decrease in sodium (Na^+), potassium (K^+) density decreases the volumetric expansion [51].

The creation of a zeolite barrier with aluminium (Al) adsorption reduces the silica dissolving rate from the aggregates on the reactive silica surface, the swelling of the ASR gel, the pore structure, and the permeability of the concrete [52–56].

The chemical formations of the basalt based aggregate specimens were determined by EDX and their results are shown in Table 6.

Table 6. Chemical composition of basalt based concrete mixture EDX result (% by weight) Mean values with standard deviations.

Specimens	Ca	Si	Al	Na	K	Fe	Ti	Mg	O	$\frac{Na+K}{Si}$	$\frac{Ca}{Si}$	$\frac{Na}{K}$
	Atom %											
BBC	**19.5**	**11.0**	**3.3**	**1.9**	**0.4**	**1.8**	**-**	**0.3**	**46.3**	**0.20**	1.77	4.95
BBC20FA	6.8	15.3	8.0	1.5	0.3	0.3	.08	.04	67.0	0.12	0.44	4.62
ASR[1]	5.3	20.9	0.4	1.4	3.2	0.1	-	-	68.6	0.22	0.36	0.46
ASR[2]	4.5	19.4	-	2.8	3.7	0.5	-	-	69.0	0.34	0.23	0.76
ASR[3]	4.5	19.9	-	0.8	3.6	-	-	-	71.2	0.26	0.25	0.61

[1,2,3]ASR: ASR concrete (Leeman et.al. 2011)

When the EDX analyses of BBC20FA and BBC specimens were compared according to the table, it was determined that fly ash substitution decreased the calcium, sodium and potassium amounts and increased the amount of aluminium. For this case, it is possible to say that the fly ash substitution reduces the volumetric expansion and the cracks associated with it.

When the EDX analysis results were compared to the ASR concrete specimens in the study of Leeman et al [44], the fact that the ratio of total alkali amount to silicate (Na-K)/Si of the test specimens is low and the calcium-silicate ratio is high in Ca/Si indicates that ASR products are not formed. In addition, the dramatic reduction of the Ca/Si ratio in the environment from 1.77 to 0.44 by the fly ash substitution is an indication that it contributes to the increase in strength.

Sodium analysis with EDX is unreliable due to evaporation, but there is no significant sodium. The low Na content of BBC20FA indicates low permeability of the NaOH solution of the fly ash (Table 6).

Leeman et al. (2011) [49], ASR products contain low levels of Mg, Al and Fe elements. Ca/Si ratio is < 0.4. Generally, Ca increases as the alkali (Na, K) content in cement paste decreases. It varies

Preprints (www.preprints.org) | NOT PEER-REVIEWED | Posted: 5 January 2024 doi:10.20944/preprints202401.0494.v1

according to the aggregate type in the crack area filled with such products, increases the Ca/Si ratio. The approximate proportions of amorphous ASR products formed in concrete aggregates ranges from (Na + K) / Si = 0.26-0.40, Ca / Si = 0.07-0.33, Na/K =0.62-1.41[57]. Thomas [50] the composition of ASR gels identified in 7-year-old laboratory concrete and a 55-year-old concrete dam was compared to the composition of calcium-silicate hydrate (C-S-H) in the dam's concrete. The composition is diverse, although there appears to be a decent link between the alkali and calcium amounts (i.e., as the calcium content increases, the alkali content decreases). The EDX result of BBC and BBC20FA specimens was compared with the results of ASR concretes [49,50]. Comparison of (Na + K)/Si ratios and Ca/Si ratios of BBC20FA and BBC specimens with ASR concretes are given in the Figure12.

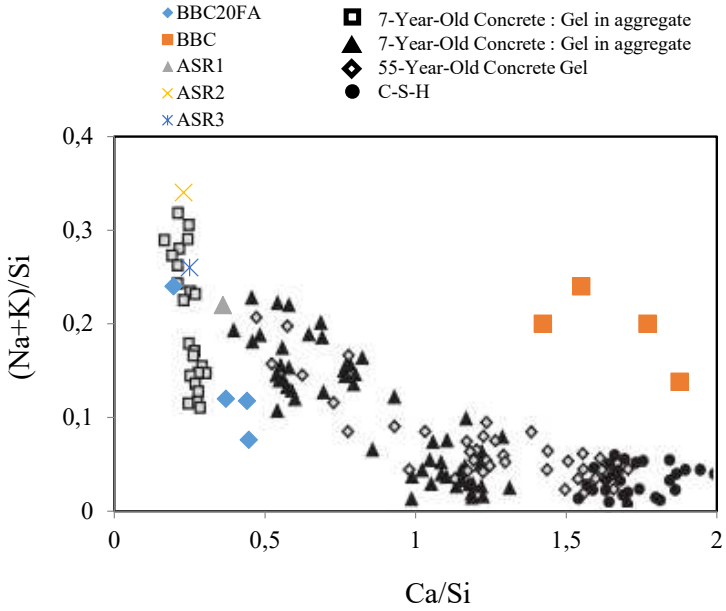

Figure 12. (Na + K)/Si-ratio of concretes BBC, BBC20FA (1M NaOH at 80° C) and ASR concretes as a function of their Ca/Si-ratio.

C-A-S-H phases supported by Si and Al in the environment from the clay matrix show that the distance from the portlandite (CH) near the origin in the Al/Ca-Si/Ca diagram shows that it is transformed into C-S-H by consuming CH (Figure 13). The highest Si/Ca group is attributed to C-S-H, the lowest Si/Ca group is attributed to portlandite (CH) [58].

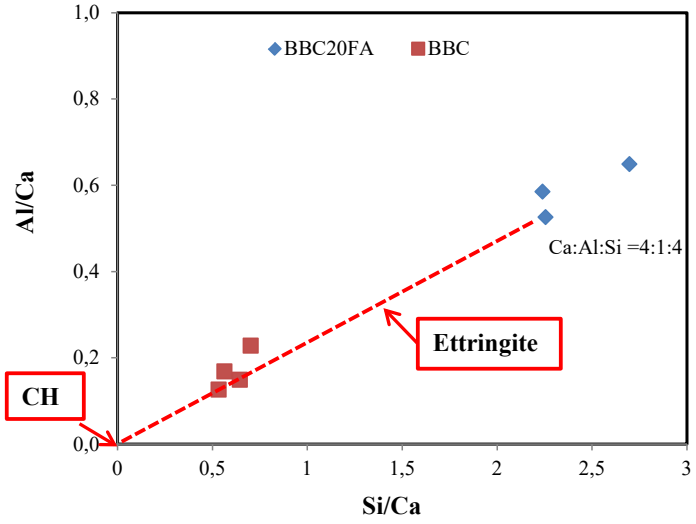

Figure 13. Atomic ratios of Al/Ca and Si/Ca for the EDX tests of C-A-S-H.

Preprints (www.preprints.org) | NOT PEER-REVIEWED | Posted: 5 January 2024 doi:10.20944/preprints202401.0494.v1

Figure 13 shows that fly ash substitution causes an increase in the C-S-H bond and the mechanical analysis results support the increase in strength with FA substitution.

3.2.3. X-Ray Diffraction (XRD)

XRD analyses of basalt aggregate specimens offer a very rich phase diversity. XRD analysis showed that the aggregate used was igneous rock, supporting the chemical analysis. Albite ($NaAlSi_3O_8$)[59] , which has a high silica content, Diopside ($MgCaSi_2O_6$)[59,60] which is found in high-silica basic and ultrabasic magmatic rocks, Microcline ($KAlSi_3O_8$) mineral, an important magmatic rock common in granites and pegmatites [61], Alabandite ($Mn^{2+}S$) and There were rare Beryllium (Be) and Anorthite ($CaAl_2Si_2O_8$) on earth [62,63]. It was also present in peaks belonging to sodium sulphate water. Accordingly, there were also peaks belonging to Halite (H) salts. Hydration products included peaks of Portlandite (P), Calcite (C), Ettringite (E) and Quartz (Q).

XRD analysis of cement-based mortars has a halo with a maximum at $2\theta \approx 25^{o}$, which is typical for amorphous silica a-SiO_2 [13,64]. This halo continues to be seen after ASR, but as ASR continues, the maximum of the halo is found to shift towards higher 2θ values. The shift of the maximum halos obtained by XRD is a good fingerprint to follow the ASR of a-SiO_2 The XRD pattern for the four gel samples is displayed in Figure 14. The reflection that is highest at $2\theta = 26^{o}$ could be linked to the typical reflection found in amorphous silicates between 24^{o} and 31^{o}.

After ASR, this halo is still visible, but as ASR goes on, it is observed that the maximum halo is shifting towards higher 2θ values. The XRD shift of the maximum halos is a useful fingerprint for tracking the a-SiO_2 ASR [64]. The XRD pattern for four gel samples is displayed in Figure 14. In amorphous silicates, the reflection typically observed between 24^{o} and 31^{o} can be correlated with the strongest reflection at $2\theta \approx 26^{o}$.

[65]. XRD traces of four ASR gels [13] were compared with the samples used in the study.

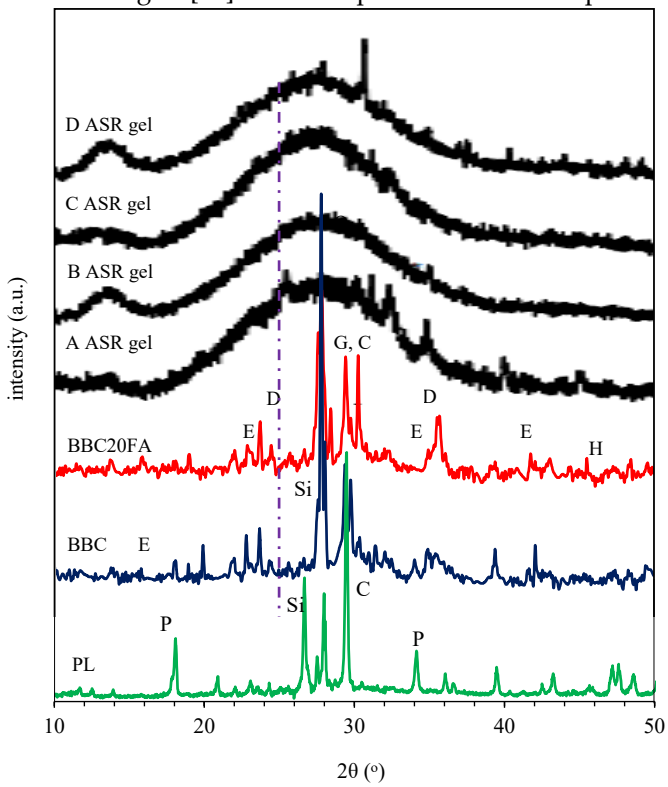

Figure 14. X-ray diffraction patterns of the four kinds of ASR gel and PL, BBC, BBC20FA **(**C= Calcite, D= Diopside E=Ettringite, H=Halite, P=Portlandite, Si= Silicon dioxide).

3.2.4. FT-IR

Preprints (www.preprints.org) | NOT PEER-REVIEWED | Posted: 5 January 2024 doi:10.20944/preprints202401.0494.v1

FTIR spectroscopy is a useful, simple application for detecting chemical bonds and determining chemical combinations within any material. BBC and BBC20FA prepared with basalt aggregate were compared with the ASR gel product in the study of Tambelli et al. (2006) [13] by FTIR analysis.

The ASR-caused cracks in the Furnas hydroelectric Rio Grande dam (Minas Gerais, Brazil) are where the ASR gel specimens were taken from. Over the course of several years, the gel specimens spontaneously emerged from the drain gallery walls and formed hard pieces with typical volumes of around 1 cm^3 [13]. FT-IR analysis of the ASR gel [13] and PL, BBC, BBC20FA from the Furnas hydroelectric dam is shown comparatively in Figure 15.

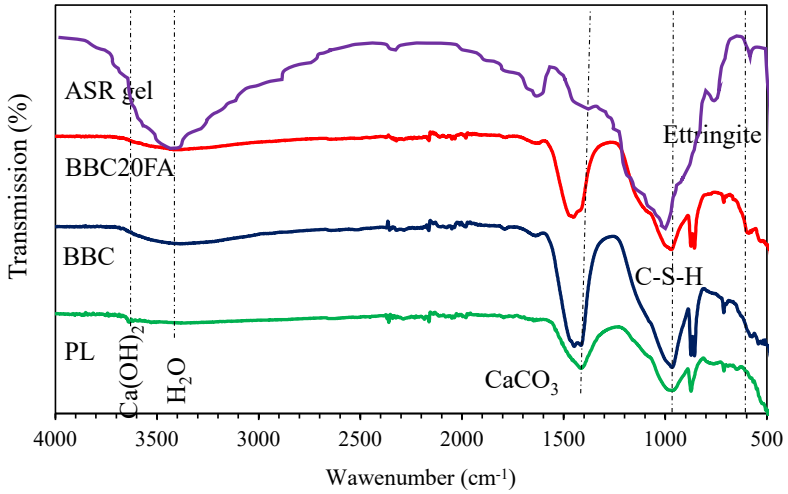

Figure 15. FTIR analysis of PL, BBC, BBC20FA and ASR gel.

According to the FI-IR spectrum Fig15, the ASR gel peaks are very different from the concrete samples. It also showed that the use of fly ash and fine volcanic aggregates in concrete caused a significant increase in calcite and C-S-H peaks.

Data from the literature can be used to attribute the detected bands. Numerous bands are connected to the amorphous silica: Si–O–X stretching where X = K or Na (953 cm^{-1}), as well as asymmetric and symmetric stretch Si–O (1154 and 1037 cm^{-1}, respectively). O-Si-O bending (457–600 cm^{-1}) and symmetric stretch (783 cm^{-1}) [66–68]. The bending of H_2O in the band from 1642 to 1660 cm^{-1} indicates the presence of molecular water. Additionally, stretching of X–OH, where X = H or Si, is linked to the broad band that spans 2300–3700 cm^{-1}, suggesting that there are a significant number of OH groups present in the silica matrix [13,69]. However, the band at 1470 cm^{-1} indicates the existence of carbonates because it corresponds to CO_3^{2-}anions [70].

Table 6. Summarized data of Figure 15.

Wave number range (cm^{-1})	Assignment	Compound formation	References
530-558	Si-O out of plane bending	Ettringite	[71–73]
882-890	CO_3^{2-}	Carbonates	[73]
969-1004	Si-O stretching and vibration	C-S-H	[71,73–75]
1520-1524	CO_3^{2-}	Calcium carbonate	[74,75]
1636-1646	H-O-H	-	[73,76]
1640-1650	C-H bending	Chemically bonded water	[73,76]
3200-3400	O-H	H_2O	[74,77]
3618-3627	O-H	Portlandite	[72,74]

3.2.5. Thermogravimetric and Differential Thermal Analysis (TGA/ DTA)

The free water still present in the specimens is transported up to approximately 100 °C. Water loss occurs in concrete between 100–250 °C (Peak1). It should be mentioned that the water in concrete is composed of three different types: chemically bonded water found in calcium hydroxide (CH),

Preprints (www.preprints.org) | NOT PEER-REVIEWED | Posted: 5 January 2024 doi:10.20944/preprints202401.0494.v1

calcium silicate hydrate (C-S-H), and capillary water. Capillary water and physically absorbed water occupy most of the weight of the cement paste, and most of the C-S-H origin water is expelled from the concrete by evaporation when the ambient temperature is above 250 °C. Additionally, CH transformation at 450 °C causes a significant mass loss. Between 450 and 550 °C, portlandite decomposes into free lime (dihydroxylation) [78–80]. A weak endothermic peak at 650 °C is attributed to the decomposition of calcite. Platret (2002) [80] found that between 600 and 700 °C, C–S–H decomposes to form β-C_2S in his study. The specimen heated at 750 °C shows the complete conversion of CH and $CaCO_3$ to CaO [81,82].

According to recent studies, the use of fly ash and fine volcanic aggregates in concrete increases the production of calcite, secondary C-S-H and C-S-A-H, which improves the matrix microstructure and increases the compressive strength. [9,83–86]. Losses due to $Ca(OH)_2$ and $CaCO_3$ were evident in the PL sample, while no sharp peaks were observed in the basalt-based samples Fig 16.

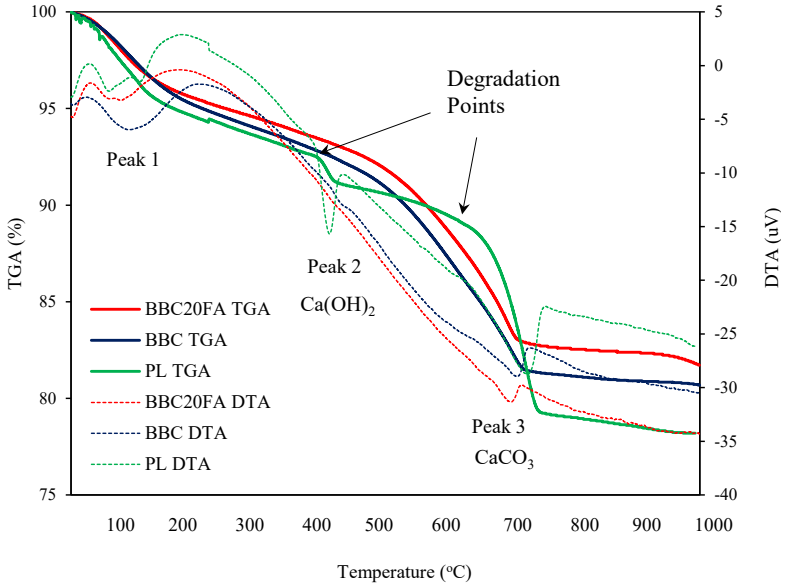

Figure 16. Thermogravimetric analysis (TGA and DTA) of specimens heated at various temperatures.

According to Figure 16, the losses due to $Ca(OH)_2$ and $CaCO_3$ were evident in the PL specimen, while no sharp peaks were observed in the basalt-based specimens. mass losses were found to be 19.31, 18.29, 21.80 % in BBC, BBC20FA, PL specimens, respectively. this result indicates that basalt aggregate and fly ash contribute to the formation of C-S-H in the strength process.

5. Conclusions

February 6, 2023 Kahramanmaraş, Turkey, 7.8 Mw, 7.6 Mw earthquakes. After the collapse of more than 90,000 reinforced concrete buildings [87], the issues of improving concrete quality and investigating strength and durability issues have gained importance. It is also important to investigate and utilize alternative rocks for concrete aggregate in reconstructed buildings to meet the need for raw materials.

When the chemical component values of Cizre basalt were examined, it was found that the SiO_2 amount was 50.63% and it was basic in character, in the test performed in ASTM C 1260 standards, the volumetric expansion of the basalt aggregate specimen was within the limit values ASR gels were not found with SEM and EDX in which microstructure were examined, and it was determined that Cizre basalt was not reactive to ASR in concrete. According to the XRD analysis, the use of fly ash decreased in Ettringite and CH phases, and an increase in the formation of C-S-H was detected. Therefore, it is possible to say that the use of basalt aggregate and fly ash increases the strength and durability of concrete.

With the use of fly ash, Si bound to CH, one of the hydration products, strengthened the C-S-H bond and increased the strength and durability. According to mechanical tests, 20% fly ash replacement increased the compressive strength value up to 10%. However, NaOH solution decreased the concrete strength by 3%.

It was concluded that igneous rocks showing basaltic properties in petrographic analysis can be used in the concrete industry since they are not reactive against ASR. In case reactive aggregates are used in concrete, it is possible to say that 20% fly ash replacement can be used as a measure against ASR.

It would be wrong to evaluate the decrease in the service life of concrete only economically. The inefficient use of the materials that make up the concrete brings with it environmental-ecological problems. Appropriate design of the concrete according to the environmental conditions and knowing the petrographic structure of the aggregate used will prevent the deterioration of the concrete in later ages and increase its service life. Thus, both economic and environmental deformations will be prevented.

References

1. Y.E. Erdoğan, Materials of Construction, M.E.T.U. Press, Ankara, 2002.
2. B. Baradan, Yapı Malzemesi II, D.E.Ü. Müh. Fak. Yay, İzmir, 2004.
3. Ö. Andiç-Çakır, Investigation of Test Methods on Alkali Aggregate Reaction, Ege University Institute of Science, 2007.
4. R. Kambiz, Alkali-silica reaction in concrete a review, in: In Proceedings of the 2013 Ready Concrete Congress, İstanbul, 2013: pp. 289–311.
5. T. Katayama, A Crıtıcal Revıew of Carbonate Rock Reactıons-Is Theır Reactıvıty Useful Or Harmful ?, 1992.
6. T. Katayama, Alkali Aggregate Reaction In The Vicinity Of Izmir, Western Turkey, Alkali Aggregate Reaction In Concrete, in: Proceedings of 11th International Conference, Canada, 2000.
7. F. Rajabipour, E. Giannini, C. Dunant, J.H. Ideker, M.D.A. Thomas, Alkali-silica reaction: Current understanding of the reaction mechanisms and the knowledge gaps, Cem Concr Res. 76 (2015) 130–146. https://doi.org/10.1016/j.cemconres.2015.05.024.
8. T. Ichikawa, M. Miura, Modified model of alkali-silica reaction, Cem Concr Res. 37 (2007) 1291–1297. https://doi.org/10.1016/j.cemconres.2007.06.008.
9. A. Karasin, M. Hadzima-Nyarko, E. Işık, M. Doğruyol, I.B. Karasin, S. Czarnecki, The Effect of Basalt Aggregates and Mineral Admixtures on the Mechanical Properties of Concrete Exposed to Sulphate Attacks, Materials. 15 (2022). https://doi.org/10.3390/ma15041581.
10. A. Leemann, P. Lura, E-modulus of the alkali-silica-reaction product determined by micro-indentation, Constr Build Mater. 44 (2013) 221–227. https://doi.org/10.1016/j.conbuildmat.2013.03.018.
11. T. Katayama, Petrographic Study of the Alkali-aggregate Reactions in Concrete, Grad. Sch. Sci. Univ. Tokyo, Dep. Earth Planet. Sci, . (2012).
12. Z. Shi, A. Leemann, D. Rentsch, B. Lothenbach, Synthesis of alkali-silica reaction product structurally identical to that formed in field concrete, Mater Des. 190 (2020). https://doi.org/10.1016/j.matdes.2020.108562.
13. C.E. Tambelli, J.F. Schneider, N.P. Hasparyk, P.J.M. Monteiro, Study of the structure of alkali-silica reaction gel by high-resolution NMR spectroscopy, J Non Cryst Solids. 352 (2006) 3429–3436. https://doi.org/10.1016/j.jnoncrysol.2006.03.112.
14. M Imaoka,. H. Hasegawa, I.Yasui. X-ray dıffractıon study of the structure of sılıcate glasses. Iı: alkalı dısılıcate glasses., (1983).
15. T.E. Stanton, Influence of cement and aggregate on concrete expansion, Eng. NewsRecord. 1, 1940.
16. A. Mohammadi, E. Ghiasvand, M. Nili, Relation between mechanical properties of concrete and alkali-silica reaction (ASR); a review, Constr Build Mater. 258 (2020). https://doi.org/10.1016/j.conbuildmat.2020.119567.
17. J. Duchesne, M. A. Bérubé, The effectiveness of supplementary cementing materials in suppressing expansion due to ASR: another look at the reaction mechanisms part 2: pore solution chemistry. , 24(2), 221-230, Cem Concr Res. 24 (1994) 221–230.
18. B Fournier, M. A Bérubé, K. J.F olliard, M. Thomas, Report on the diagnosis, prognosis, and mitigation of Alkali-Silica Reaction (ASR) in transportation structures (No. FHWA-HIF-09-004). , 2010.
19. M.A. Bérubé, C. Tremblay, B. Fournier, M.D. Thomas, D.B. Stokes, Influence of lithium-based products proposed for counteracting ASR on the chemistry of pore solution and cement hydrates, Cem Concr Res. 34 (2004) 1645–1660. https://doi.org/10.1016/j.cemconres.2004.03.025.

20. S. Poyet, A. Sellier, B. Capra, G. Foray, J.M. Torrenti, H. Cognon, E. Bourdarot, Chemical modelling of Alkali Silica reaction: Influence of the reactive aggregate size distribution, Materials and Structures/Materiaux et Constructions. 40 (2007) 229–239. https://doi.org/10.1617/s11527-006-9139-3.
21. S.A. Mohammad Shahidul Islam, A Critical Assessment to the Performance of Alkali-Silica Reaction (ASR) in Concrete, Can Chem Trans. (2013) 253–266. https://doi.org/10.13179/canchemtrans.2013.01.04.0026.
22. M. Kawamura, H. Fuwa, Effects of lithium salts on ASR gel composition and expansion of mortars, Cem Concr Res. 33 (2003) 913–919. https://doi.org/10.1016/S0008-8846(02)01092-X.
23. T. Kurihara, K Katawaki, Effects of moisture control and inhibition on alkali silica reaction, in: 8th ICAAR, International Conference on Alkali Aggregate Reactions, Kyoto , 1989: pp. 629–634.
24. D. W Hobbs, J. Bensted, P. Barnes, Alkali–Silica Reaction in Concrete, in: Structure and Performance of Cement, 2002: pp. 265–281.
25. F. Gaboriaud, D. Chaumont, A. Nonat, A. Craeivich, Study of the Influence of Alkaline Ions (Li, Na and K) on the Structure of the Silicate Entities in Silico Alkaline Sol and on the Formation of the Silico-Calco-Alkaline Gel, 1998.
26. F Gaboriaud, A., Nonat, D. Chaumont, A.Craievich, Aggregation and gel formation in basic silico-calco-alkaline solutions studied: a SAXS, SANS, and ELS study, , J Phys Chem B. (1999) 5775–5781.
27. S. Diamond, ASR — another look at mechanisms, Proc., in: 8th International Conf. on Alkali–Aggregate Reaction (ICAAR), Kyoto, 1989: pp. 83–94.
28. E.O. Fanijo, J.T. Kolawole, A. Almakrab, Alkali-silica reaction (ASR) in concrete structures: Mechanisms, effects and evaluation test methods adopted in the United States, Case Studies in Construction Materials. 15 (2021). https://doi.org/10.1016/j.cscm.2021.e00563.
29. B. Baradan, H. Yazici, H. Ün, Betonarme Yapılarda Kalıcılık(Durabilite)., D.E.Ü. Müh. Fak. Yayın, 2002.
30. C. Tremblay, M.A. Bérubé, B. Fournier, M.D. Thomas, K.J. Folliard, Experimental investigation of the mechanisms by which LiNO3 is effective against ASR, Cem Concr Res. 40 (2010) 583–597. https://doi.org/10.1016/j.cemconres.2009.09.022.
31. R.W. le Maitre, A classification of Igneous Rocks and Glossary of Terms, Blackwell Scientific Publ, Oxford, UK, 1989.
32. P. Hagelia, I. Fernandes, ON THE AAR SUSCEPTIBILITY OF GRANITIC AND QUARTZITIC AGGREGATES IN VIEW OF PETROGRAPHIC CHARACTERISTICS AND ACCELERATED TESTING, n.d.
33. M.H. Shehata, M.D.A. Thomas, R.F. Bleszynski, The effects of fly ash composition on the chemistry of pore solution in hydrated cement pastes, 1999.
34. P. Kumar Mehta, P.J. M Monteiro, Concrete: Microstructure, Properties, and Materials, Fourth Edition, n.d.
35. BS EN 196-6, BS EN 196-6:2018 Methods of testing cement is classified in these ICS categories: 91.100.10 Cement. Gypsum. Lime. Mortar, 2018.
36. ASTM 204, Standard Test Methods for Fineness of Hydraulic Cement by Air-Permeability Apparatus, (2013).
37. Standard, B. 8007: Design of concrete structures for retaining aqueous liquids. BSI, London, UK., 1987.
38. ASTM (American Society for Testing and Materials) Standards (2006a) Standard test method for the resistance to degradation of small-size coarse aggregates by abrasion and impact in the Los Angeles Machine, C131–03, v. 04.02, USA, 2006.
39. ASTM Standard Standard Test Method for Tensile Strength of Monolithic Advanced Ceramics at Ambient Temperatures, C 1273-05. Annual Book of ASTM Standards, Vol. 15.01, American Society of Testing and Materials, Philadelphia, PA., 2005.
40. B.G. Kutchko, A.G. Kim, Fly ash characterization by SEM-EDS, Fuel. 85 (2006) 2537–2544. https://doi.org/10.1016/j.fuel.2006.05.016.
41. R.T. Chancey, P. Stutzman, M.C.G. Juenger, D.W. Fowler, Comprehensive phase characterization of crystalline and amorphous phases of a Class F fly ash, Cem Concr Res. 40 (2010) 146–156. https://doi.org/10.1016/j.cemconres.2009.08.029.
42. X. Li, X. Ma, S. Zhang, E. Zheng, Mechanical properties and microstructure of class C fly ash-based geopolymer paste and mortar, Materials. 6 (2013) 1485–1495. https://doi.org/10.3390/ma6041485.
43. P. Duxson, A. Fernández-Jiménez, J.L. Provis, G.C. Lukey, A. Palomo, J.S.J. Van Deventer, Geopolymer technology: The current state of the art, J Mater Sci. 42 (2007) 2917–2933. https://doi.org/10.1007/s10853-006-0637-z.
44. M.L. Granizo, S. Alonso, M.T. Blanco-Varela, A. Palomo, Alkaline activation of metakaolin: Effect of calcium hydroxide in the products of reaction, in: Journal of the American Ceramic Society, American Ceramic Society, 2002: pp. 225–231. https://doi.org/10.1111/j.1151-2916.2002.tb00070.x.
45. C.K. Yip, J.S.J. Van Deventer, Microanalysis of calcium silicate hydrate gel formed within a geopolymeric binder, n.d.
46. S.-D. Wang, K.L. Scrivener, P.L. Pratt, 0008-8846(94) 00046-8 FACTORS AFFECTING THE STRENGTH OF ALKALI-ACTIVATED SLAG, 1994.

47. ASTM C 1260, "Standart Test Method for Potential Alkali Reactivity of Aggregates (Mortar-Bar Method)", Annual Book of ASTM Standarts, , Philadelphia, USA., n.d.
48. B. Middendorf, J.J. Hughes, K. Callebaut, G. Baronio, I. Papayianni, Investigative methods for the characterisation of historic mortars - Part 1: Mineralogical characterisation, Materials and Structures/Materiaux et Constructions. 38 (2005) 761–769. https://doi.org/10.1617/14281.
49. A. Leemann, G. le Saout, F. Winnefeld, D. Rentsch, B. Lothenbach, Alkali-Silica reaction: The Influence of calcium on silica dissolution and the formation of reaction products, Journal of the American Ceramic Society. 94 (2011) 1243–1249. https://doi.org/10.1111/j.1551-2916.2010.04202.x.
50. M.l Thomas, The role of calcium hydroxide in alkali recycling in concrete, in: J. Skalny, J. Gebauer, I. Odler (Eds.), Materials Science of Concrete Special Volume on Calcium Hydroxide in Concrete, American Ceramic Society, Westerville, OH 2001, pp. 269–280., In Materials Science of Concrete Special Volume on Calcium Hydroxide in Concrete. (2001) 269–280.
51. S. Urhan, Alkali silica and pozzolanic reactions in concrete. Part 1: interpretation of published results and an hypothesis concerning the mechanism, Cement Concrete Research. 17 (1987) 141–152.
52. R.K. Iler, Effect of Adsorbed Alumina on the Solubility of Amorphous Silica in Water, n.d.
53. S.-Y. Hong, F.P. Glasser, Alkali sorption by C-S-H and C-A-S-H gels Part II. Role of alumina, n.d.
54. K.J. Hünger, The contribution of quartz and the role of aluminum for understanding the AAR with greywacke, Cem Concr Res. 37 (2007) 1193–1205. https://doi.org/10.1016/j.cemconres.2007.05.009.
55. T. Chappex, K.L. Scrivener, The effect of aluminum in solution on the dissolution of amorphous silica and its relation to cementitious systems, Journal of the American Ceramic Society. 96 (2013) 592–597. https://doi.org/10.1111/jace.12098.
56. T. Chappex, K. Scrivener, Alkali fixation of C-S-H in blended cement pastes and its relation to alkali silica reaction, Cem Concr Res. 42 (2012) 1049–1054. https://doi.org/10.1016/j.cemconres.2012.03.010.
57. K.J. Hünger, The contribution of quartz and the role of aluminum for understanding the AAR with greywacke, Cem Concr Res. 37 (2007) 1193–1205. https://doi.org/10.1016/j.cemconres.2007.05.009.
58. I. García Lodeiro, A. Fernández-Jimenez, A. Palomo, D.E. Macphee, Effect on fresh C-S-H gels of the simultaneous addition of alkali and aluminium, Cem Concr Res. 40 (2010) 27–32. https://doi.org/10.1016/j.cemconres.2009.08.004.
59. MTA, General Directorate of Mineral Research And Exploration , Ankara, Turkey, n.d.
60. M M Smedskjaer; M Jensen; Y-Z Yue, Theoretical calculation and measurement of the hardness of diopside, Journal of the American Ceramic Society. Doi:10.1111/j.1551-2916.2007.02166. 91 (2) (2008) 514–518.
61. L.N. Warr, IMA–CNMNC approved mineral symbols, Mineral Mag. 85 (2021) 291–320. https://doi.org/10.1180/mgm.2021.43.
62. Puchta R., A brighter beryllium , Nature Chemistry,Https://Doi.Org/10.1038/Nchem.1033. 3(5), 416. (2011).
63. W. A. Deer, R. A. Howie, J. Zussman, An Introduction to the Rock Forming Minerals. ISBN 0-582-44210-9., 1966.
64. A. Hamoudi, L. Khouchaf, C. Depecker, B. Revel, L. Montagne, P. Cordier, Microstructural evolution of amorphous silica following alkali-silica reaction, J Non Cryst Solids. 354 (2008) 5074–5078. https://doi.org/10.1016/j.jnoncrysol.2008.07.001.
65. M. Imaoka, H. Hasegawa, I.Yasui,, X-ray diffraction study of the structure of silicate glasses. II. alkali disilicate glasses., Physics and Chemistry of Glasses. (1983).
66. J. Serra, P. González, S. Liste, C. Serra, S. Chiussi, B. León, M. Pérez-Amor, H.O. Ylänen, M. Hupa, FTIR and XPS studies of bioactive silica based glasses, J Non Cryst Solids. 332 (2003) 20–27. https://doi.org/10.1016/j.jnoncrysol.2003.09.013.
67. H. Takadama, H.M. Kim, T. Kokubo, T. Nakamura, Mechanism of biomineralization of apatite on a sodium silicate glass: TEM-EDX study in vitro, Chemistry of Materials. 13 (2001) 1108–1113. https://doi.org/10.1021/cm0008718.
68. T. Uchino, T. Sakka, K. Hotta, M. Lwasaki, Attenuated Total Reflectance Fourier-Transform Infrared Spectra of a Hydrated Sodium Silicate Glass, 1989.
69. F.X., and D.J.Kiemle. Webster, Spectrometric identification of organic compounds. ., John Wiley & Sons, 2005.
70. S. Ricol, E. Vernaz, P. Barboux, Synthesis of Gels in the System Na20-ZrO2-SiO2, Kluwer Academic Publishers, 1997.
71. Y. Ping, R.J. Kirkpatrick, P. Brent, P.F. McMillan, X. Cong, Structure of calcium silicate hydrate (C-S-H): Near-, mid-, and far-infrared spectroscopy, Journal of the American Ceramic Society. 82 (1999) 742–748. https://doi.org/10.1111/j.1151-2916.1999.tb01826.x.
72. M. Singh, S. Waghmare, S. Vinodh Kumar, Characterization of lime plasters used in 16th century Mughal monument, J Archaeol Sci. 42 (2014) 430–434. https://doi.org/10.1016/j.jas.2013.11.019.
73. R. Choudhary, R. Gupta, R. Nagar, Impact on fresh, mechanical, and microstructural properties of high strength self-compacting concrete by marble cutting slurry waste, fly ash, and silica fume, Constr Build Mater. 239 (2020). https://doi.org/10.1016/j.conbuildmat.2019.117888.

74. M. Chollet, M. Horgnies, Analyses of the surfaces of concrete by Raman and FT-IR spectroscopies: Comparative study of hardened samples after demoulding and after organic post-treatment, Surface and Interface Analysis. 43 (2011) 714–725. https://doi.org/10.1002/sia.3548.
75. M. Horgnies, P. Willieme, O. Gabet, Influence of the surface properties of concrete on the adhesion of coating: Characterization of the interface by peel test and FT-IR spectroscopy, Prog Org Coat. 72 (2011) 360–379. https://doi.org/10.1016/j.porgcoat.2011.05.009.
76. P.A. Bhat, N.C. Debnath, Theoretical and experimental study of structures and properties of cement paste: The nanostructural aspects of CSH, Journal of Physics and Chemistry of Solids. 72 (2011) 920–933. https://doi.org/10.1016/j.jpcs.2011.05.001.
77. M., Horgnies, J. J., Chen, C. Bouillon, Overview about the use of Fourier transform infrared spectroscopy to study cementitious materials. , 77th ed., WIT Trans. Eng. Sci, 2013.
78. Z. P Bažant, M. F. Kaplan, Z.P.Bazant, Concrete at high temperatures: material properties and mathematical models., 1996.
79. A. Noumowe, Effet de hautes températures (20-600 C) sur le béton: cas particulier du béton a hautes performances (Doctoral dissertation, , INSA)., 1995.
80. G. Platret, Suivi de l'hydratation du ciment et de l'évolution des phases solides dans les bétons par analyse thermique, caractéristiques microstructurales et propriétés relativesa la durabilité des bétons. , 2002.
81. B. Zhang, Effects of moisture evaporation (weight loss) on fracture properties of high performance concrete subjected to high temperatures, Fire Saf J. 46 (2011) 543–549. https://doi.org/10.1016/J.FIRESAF.2011.07.010.
82. A. Savva, P. Manita, K.K. Sideris, Influence of elevated temperatures on the mechanical properties of blended cement concretes prepared with limestone and siliceous aggregates, Cem Concr Compos. 27 (2005) 239–248. https://doi.org/10.1016/J.CEMCONCOMP.2004.02.013.
83. J. Moon, S. Bae, K. Celik, S. Yoon, K.H. Kim, K.S. Kim, P.J.M. Monteiro, Characterization of natural pozzolan-based geopolymeric binders, Cem Concr Compos. 53 (2014) 97–104. https://doi.org/10.1016/j.cemconcomp.2014.06.010.
84. K. Kupwade-Patil, S.D. Palkovic, A. Bumajdad, C. Soriano, O. Büyüköztürk, Use of silica fume and natural volcanic ash as a replacement to Portland cement: Micro and pore structural investigation using NMR, XRD, FTIR and X-ray microtomography, Constr Build Mater. 158 (2018) 574–590. https://doi.org/10.1016/j.conbuildmat.2017.09.165.
85. K. Annaba, Y. El Mendili, H. Stout, A. Ech-chebab, B. Ouaki, M. Cherkaoui, C. Florence, Mechanical, electrochemical (EIS), and microstructural characterization of reinforced concrete incorporating natural volcanic pozzolan, Case Studies in Construction Materials. 19 (2023). https://doi.org/10.1016/j.cscm.2023.e02620.
86. A. Karaşin, M. Doğruyol, An experimental study on strength and durability for utilization of fly ash in concrete mix, Advances in Materials Science and Engineering. 2014 (2014). https://doi.org/10.1155/2014/417514.
87. 2023 Kahramanmaraş depremleri- Vikipedi, (n.d.). https://tr.wikipedia.org/wiki/2023_Kahramanmara%C5%9F_depremleri (accessed December 3, 2023)., (2023).